Dalton Transactions

ROYAL SOCIETY OF CHEMISTRY

PAPER

View Article Online
View Journal | View Issue

Cite this: *Dalton Trans.*, 2020, **49**, 438

Photophysical properties of some novel tetraphenylimidazole derived BODIPY based fluorescent molecular rotors†

Bhupendra Kumar Dwivedi, Vishwa Deepak Singh, Yogesh Kumar and Daya Shankar Pandey *

Received 28th October 2019,
Accepted 27th November 2019

DOI: 10.1039/c9dt04177j

rsc.li/dalton

The strategic design, synthesis and thorough characterization of four novel hydroxyl-substituted tetraphenylimidazole (HPI) based boron dipyrromethene (BODIPY) fluorophores (**HPIB1–HPIB4**) have been reported. Single crystal X-ray structure determination unveiled non-planar twisted orientations for these molecules. The non-planar orientations entirely restrict detrimental π–π interactions and avoid the non-radiative relaxation pathway for excited states in the solid/aggregated state and make them AIE active. The AIE characteristics of these compounds have been related to fine J-aggregation (evident from their crystal structures) along with restricted intra-molecular rotations (RIRs). These compounds display significant sensitivity toward viscosity and can serve as fluorescent molecular rotors due to multiple phenyl groups around the imidazole ring, which has been confirmed by measuring fluorescence quantum yields and lifetimes.

Introduction

Fluorescent organic materials have fascinated the scientific community because of their utility in various areas including biology, chemistry, materials science, *etc*.[1] The majority of organic fluorophores display fluorescence quenching (ACQ) in the aggregated state or viscous medium which limits their possible applications in diverse areas.[2] In this context, aggregation-induced emission (AIE) has been attractive as it overcomes ACQ and makes the system highly emissive in the aggregated state.[3] The photophysical properties of planar luminogens may be controlled by adopting various strategies[4] including introduction of bulky rotors,[5] charge transfer[6] and excited-state intramolecular proton transfer[7] (ESIPT) properties. Introduction of rigid and bulky aromatic units as rotors can be a good move toward converting ACQ systems into AIE fluorophores.[5] Essentially, dynamic intramolecular motions/rotations of the bulky and rigid aromatic core utilize the major fraction of the excitation energy and make it non- or weakly emissive in dilute solution. However, in the aggregated state or viscous medium suppression of the active motions/molecular rotations increases radiative channels and therefore leads to the enhancement of the fluorescence intensity.[5] Furthermore, intramolecular H-bonding also enhances the emission properties of the compounds in dilute solution and in the aggregated state by inducing planarity in the systems.[7]

An extensive literature survey on the emission behavior of AIE materials revealed the prominent role of J-aggregation which not only boosts the emission but also causes shifts of the emission maxima to long wavelengths (red/NIR region).[8] Thus to develop systems with J-type molecular packing, it is essential to modify the molecules in such a way that they adopt non-planar orientations and boost quantum efficiency in the aggregated state. Furthermore, the utility of various organic fluorophores with a variety of functionalities exhibiting AIE has been explored.[3] Among these, BODIPYs have fascinated researchers due to their excellent properties and applications in diverse areas.[9] Usually the quantum efficiencies of the BODIPYs are high in dilute solution; however, they suffer from fluorescence quenching in the aggregated state.[8c,10] These compounds hardly fluoresce in the solid state due to ACQ arising from π–π stacking in dense medium.[3,11] In this direction, in order to suppress detrimental π–π stacking, Tang *et al.* introduced a known AIE system tetraphenylethylene (TPE) into the BODIPY core.[12a,b] The triphenylamine (TPA) system has also been integrated into the BODIPY core to achieve emission in the solid/aggregated state.[12c,d] These systems motivated the design of the BODIPYs possessing bulky phenyl groups which can show non-planar orientations and avoid detrimental π–π stacking in the aggregated state.[12] Furthermore, multiple bulky phenyl rotors linked *via* single

Department of Chemistry, Institute of Science, Banaras Hindu University, Varanasi - 221 005, UP, India. E-mail: dsprewa@yahoo.com, dspbhu@bhu.ac.in

†Electronic supplementary information (ESI) available: CCDC 1945394–1945397. For ESI and crystallographic data in CIF or other electronic format see DOI: 10.1039/C9DT04177J

bonds may cause viscosity-dependent emission changes and can serve as fluorescent molecular rotors (FMRs). Viscosity is an important parameter that determines the diffusion rate of a species in various environments. Also, minute viscosity changes are related to diseases and malfunctions at the cellular level in biological systems.[13] Thus, such molecular rotors may play a vital role in viscosity sensing in various environments and biological systems including subcellular organelles and related processes.[13]

Considering these points, in this work, four BODIPY fluorophores based on hydroxyl-substituted tetraphenylimidazole (HPI) derivatives have been described. It is presumed that the phenyl rotors of HPI may favor radiative decay pathways in the solid state or viscous medium due to the suppression of active intramolecular rotations and the compounds may serve as FMRs. The phenyl rotors may also facilitate the entire molecule to lose planarity and enable it to avoid detrimental π–π stacking and display appropriate interactions causing J-aggregates required for good emission in the aggregated state. Herein, we present the efficient AIE, good solid state fluorescence, and impressive viscosity-dependent emission behavior of hydroxyl-substituted tetraphenylimidazole based BODIPY fluorophores.

Experimental details

Reagents

Solvents were dried and distilled following literature procedures prior to use.[14] Reagents like benzil, aniline, *p*-toluidine, 4-chloroaniline, 2-amino-5-nitrobenzophenone, hexamine, triethylamine, salicylaldehyde, 5-chlorosalicylaldehyde, trifluoroacetic acid, pyrrole, 2,3-dichloro-5,6-dicyano-1,4-benzoquinone (DDQ), and boron trifluoride diethyletherate were purchased from Sigma Aldrich, India and used as received.

General information

^{1}H [500 MHz; $(CH_3)_4Si$], ^{11}B [160.4 MHz; $BF_3{\cdot}OEt_2$], ^{13}C [125 MHz; $(CH_3)_4Si$] and ^{19}F [470.6 MHz; CF_3COOH] NMR spectra were acquired on a JEOL AL 500 FT-NMR spectrometer at room temperature. Electrospray ionization mass spectroscopy (ESI-MS) studies were performed on an Agilent Technologies (1260 Infinity) mass spectrometer. Elemental analyses (C, H, and N) were performed on an Elementar Vario EL III Carlo Erba 1108 in the micro-analytical laboratory of the Sophisticated Analytical Instrumentation Facility (SAIF), Central Drug Research Institute (CDRI), Lucknow, India. Electronic absorption spectra were acquired on a Shimadzu UV-1800 and fluorescence spectra on a PerkinElmer LS 55 spectrometer. Field emission scanning electron microscopic (FESEM) studies were performed on a Nova NanoSEM 450 scanning electron microscope. Time-resolved fluorescence (TRF) decay experiments were performed on a TCSPC system (Horiba Yovin; Delta Flex). In these studies, the samples were excited using a picosecond diode laser (Model: Delta Diode) and data analysis was performed using EzTime (Horiba Scientific) decay analysis software.

Single crystal X-ray analyses

Crystal data for **HPIB1–HPIB4** were acquired on a Bruker APEX II CCD diffractometer at room temperature with Mo-Kα radiation (λ = 0.71073 Å). The structures were solved by direct methods (SHELXS 97) and refined by full-matrix least squares on F^2 (SHELX 97) with version 2016/1 of SHELXL.[15] Non-hydrogen atoms were refined anisotropically and hydrogen atoms geometrically fixed and refined using a riding model. Interaction and stacking distances were analyzed using PLATON.[16] The CCDC deposition No. 1945394 (**HPIB1**), 1945395 (**HPIB2**), 1945396 (**HPIB3**) and 1945397 (**HPIB4**) contain supplementary crystallographic data for this paper.†

Theoretical studies

Quantum chemical calculations on **HPIB1–HPIB4** were carried out at the B3LYP Density Functional Theory (DFT) level using B3LYP/6-31G**.[17] Geometry optimization and frequency calculations were performed using the Gaussian 09 suite of programs.[18]

Syntheses

Preparation of 2-hydroxy-3-(1,4,5-triphenyl-1*H*-imidazol-2-yl)-benzaldehyde (4a). Compound **3a** (776.46 mg, 2 mmol) and an equivalent amount of hexamethylenetetramine (280.37 mg, 2 mmol) were added to a round bottom (RB) flask containing trifluoroacetic acid (10 mL). Contents of the flask were refluxed at 100 °C for 12 hours under stirring and the progress of the reaction was monitored by TLC. After complete consumption of **3a** the reaction mixture was allowed to cool to room temperature. It was then treated with 4 M HCl (30 ml) solution and stirring was continued for an additional one hour to obtain a yellow solid. The solid was washed with an excess of diethyl ether and the solid powder was subjected to column chromatography (silica gel) using dichloromethane/*n*-hexane (1 : 9) as the eluent. The first fraction afforded the desired product as a yellow solid. Yield: 400 mg (48%). **^{1}H NMR** (500 MHz, $CDCl_3$) δ = 10.41 (s, 1H), 7.63 (s, 1H), 7.52 (d, J = 7 Hz, 3H), 7.44–7.39 (m, 3H), 7.3–7.25 (m, 6H), 7.18–7.14 (m, 4H), 6.83 (s, 1H). **^{13}C NMR** (125 MHz, $CDCl_3$) δ = 190.08, 160.05, 142.14, 135.63, 134.80, 132.47, 131.23, 131.11, 130.83, 129.94, 129.91, 129.17, 129.03, 128.68, 128.49, 128.29, 128.13, 127.80, 127.10, 124.47, 123.51, 115.63 ppm.

Preparation of 5-chloro-2-hydroxy-3-(1,4,5-triphenyl-1*H*-imidazol-2-yl)-benzaldehyde (4b). Compound **4b** was prepared following the above procedure described for **4a** using **3b** (845.82 mg, 2 mmol) and hexamethylenetetramine (1122 mg; 8 mmol) in trifluoroacetic acid (15 ml) and the reaction mixture was refluxed for 36 hours at 100 °C. It was isolated as a yellow solid. Yield: 750 mg (83.16%). **^{1}H NMR** (500 MHz, $CDCl_3$) δ = 10.51 (s, 1H), 7.65 (s, 1H), 7.53 (d, J = 7 Hz, 2H), 7.47–7.42 (m, 3H), 7.31–7.25 (m, 7H), 7.21–7.16 (m, 4H), 6.74 (s, 1H). **^{13}C NMR** (125 MHz, $CDCl_3$) δ = 189.56, 160.32, 142.62, 135.97, 135.27, 131.86, 131.24, 131.17, 129.99, 129.92, 128.92, 128.79, 128.66, 128.47, 128.26, 127.64, 127.03, 124.78, 123.18, 115.62 ppm.

Preparation of 5-chloro-3-(4,5-diphenyl-1-(*p*-tolyl) -1*H*-imidazol-2-yl) -2-hydroxy-benzaldehyde (4c). This compound was prepared following the above procedure described for **4b** using **3c** (874 mg, 2 mmol). Yield: 800 mg (86.03%). **^{1}H NMR** (500 MHz, $CDCl_3$) δ = 10.29 (s, 1H), 7.63 (s, 1H), 7.50 (t, J = 2 Hz, 3H), 7.31–7.25 (m, 8H), 7.16–7.14 (m, 4H), 7.03 (d, J = 8.5 Hz, 3H), 2.34 (s, 3H). **^{13}C NMR** (125 MHz, $CDCl_3$) δ = 190.95, 159.72, 141.75, 140.27, 134.17, 133.56, 132.50, 131.32, 131.07, 130.39, 129.14, 128.83, 128.71, 128.54, 128.27, 128.06, 127.74, 127.65, 127.23, 123.95, 123.80, 115.46, 21.20 ppm.

Preparation of 5-chloro-3-(1-(4-chlorophenyl)-4,5-diphenyl-1*H*-imidazol-2-yl)-2 hydroxybenzaldehyde (4d). Compound **4d** was prepared following the above procedure described for **4b** using **3d** (915 mg, 2 mmol). Yield: 779 mg (80.24%). **^{1}H NMR** (500 MHz, $CDCl_3$) δ = 10.50 (s, 1H), 7.65 (d, J = 2.5 Hz, 1H), 7.54 (d, J = 7.5 Hz, 1H), 7.50 (d, J = 7 Hz, 2H), 7.39 (d, J = 9 Hz, 2H), 7.33–7.25 (m, 5H), 7.14–7.11 (m, 4H), 6.75 (d, J = 2.5 Hz, 1H). **^{13}C NMR** (125 MHz, $CDCl_3$) δ = 189.40, 160.21, 142.58, 135.91, 135.85, 134.68, 132.14, 131.47, 131.14, 130.22, 129.53, 129.05, 128.82, 128.76, 128.66, 128.45, 128.32, 127.94, 127.59, 126.93, 125.00, 123.44, 116.07 ppm.

Preparation of 2-(di(1*H*-pyrrol-2-yl)methyl)-6-(1,4,5-triphenyl-1*H*-imidazol-2-yl)-phenol (5a). Catalytic amounts of trifluoroacetic acid (2 drops) were added under stirring to a solution of **4a** (1666 mg, 4 mmol) in pyrrole (10.0 mL) and the reaction mixture was stirred for 12 hours at room temperature. After complete consumption of the aldehyde (ensured by TLC), the excess of pyrrole was removed under reduced pressure on a rotatory evaporator. The crude product was subjected to silica gel column chromatography (ethyl acetate/hexane, 1 : 9) to obtain **5a** as a white solid. Yield: 75.09% (1600 mg). **^{1}H NMR** (500 MHz, $CDCl_3$) δ = 8.47 (s, br, 2H), 7.50 (d, J = 7.5 Hz, 2H), 7.29–7.20 (m, 10H), 7.15 (d, J = 6.5 Hz, 2H), 7.06–7.02 (m, 3H), 6.72 (s, 2H), 6.39 (d, J = 2 Hz, 1H), 6.17 (d, J = 2.5 Hz, 2H), 6.00 (s, 2H). 5.83 (s, 1H). **^{13}C NMR** (125 MHz, $CDCl_3$) δ = 154.39, 143.87, 139.78, 135.00, 133.86, 132.65, 132.18, 131.83, 131.25, 130.97, 130.39, 129.75, 129.46, 128.56, 128.50, 128.29, 128.14, 127.18, 126.96, 124.49, 122.63, 117.02, 114.10, 108.24, 106.74, 39.27 ppm.

Preparation of 4-chloro-2-(di(1*H*-pyrrol-2-yl)methyl)-6-(1,4,5-triphenyl-1*H*-imidazol-2-yl)-phenol (5b). Compound **5b** was prepared following the above procedure for **5a** using **4b** (1804 mg, 4 mmol) in place of **4a**. Yield: 76.48% (1735 mg). **^{1}H NMR** (500 MHz, $CDCl_3$) δ = 8.47 (s, br, 2H), 7.50 (d, J = 8.5 Hz, 2H), 7.45–7.40 (m, 3H), 7.28–7.22 (m, 6H), 7.19–7.17 (m, 2H), 7.15–7.13 (m, 2H), 7.02 (d, J = 2.5 Hz, 1H), 6.72 (d, J = 1.5 Hz, 2H), 6.35 (d, J = 2 Hz, 1H), 6.16 (d, J = 3.5 Hz, 2H), 6.00 (s, 2H), 5.83 (s, 1H). **^{13}C NMR** (125 MHz, $CDCl_3$) δ = 154.39, 143.82, 136.58, 132.29, 131.81, 131.26, 130.92, 129.83, 129.62, 129.36, 128.64, 128.53, 128.32, 127.26, 126.98, 124.49, 122.66, 117.04, 113.99, 108.27, 106.76, 39.30 ppm.

Preparation of 4-chloro-2-(di(1*H*-pyrrol-2-yl)methyl)-6-(4,5-diphenyl-1-(*p*-tolyl)-1*H*-imidazol-2-yl)-phenol (5c). Compound **5c** was prepared following the above procedure for **5a** using **4c** (1860 mg, 4 mmol) in place of **4a**. Yield: 76.57% (1780 mg). **^{1}H NMR** (500 MHz, $CDCl_3$) δ = 8.44 (s, br, 2H), 7.49 (d, J = 7 Hz, 2H), 7.26–7.23 (m, 6H), 7.20 (d, J = 7.5 Hz, 2H), 7.13 (d, J = 7.5 Hz, 2H), 7.04 (d, J = 8 Hz, 2H), 7.00 (d, J = 2 Hz, 1H), 6.70 (d, J = 7 Hz, 2H), 6.39 (d, J = 2 Hz, 1H). 6.15 (d, J = 8.5 Hz, 2H), 5.98 (s, 2H), 5.82 (s, 1H), 2.38 (s, 3H). **^{13}C NMR** (125 MHz, $CDCl_3$) δ = 154.39, 143.87, 139.77, 134.99, 133.86, 132.65, 132.19, 131.82, 131.24, 130.96, 130.38, 129.72, 129.45, 128.55, 128.49, 128.28, 128.14, 127.17, 126.94, 124.48, 122.62, 117.00, 114.08, 108.23, 106.73, 39.30, 21.02 ppm.

Preparation of 4-chloro-2-(1-(4-chlorophenyl)-4,5-diphenyl-1*H*-imidazol-2-yl)-6-(di(1*H*-pyrrol-2-yl)methyl)-phenol (5d). Compound **5d** was prepared following the above procedure for **5a** using **4d** (1942 mg, 4 mmol) in place of **4a**. Yield: 80% (1920 mg). **^{1}H NMR** (500 MHz, $CDCl_3$) δ = 8.43 (s, br, 2H), 7.48 (d, J = 7 Hz, 2H), 7.40–7.38 (m, 2H), 7.32–7.22 (m, 6H), 7.12–7.11 (m, 4H), 7.04 (d, J = 3 Hz, 1H) 7.71 (d, J = 6.5 Hz, 2H), 6.41 (d, J = 2 Hz, 1H), 6.16 (d, J = 9 Hz, 2H), 5.99 (s, 2H), 5.84 (s, 1H). **^{13}C NMR** (125 MHz, $CDCl_3$) δ = 154.34, 143.81, 135.68, 135.49, 135.11, 132.57, 132.39, 131.70, 131.23, 130.82, 130.09, 130.00, 129.76, 129.11, 128.90, 128.75, 128.35, 127.39, 126.97, 124.39, 122.85, 117.08, 113.77, 108.33, 106.81, 39.18 ppm.

Preparation of 5,5-difluoro-10-(2-hydroxy-3-(1,4,5-triphenyl-1*H*-imidazol-2-yl)-phenyl)-5*H*-dipyrrolo-[1,2-c:2′,1′-f][1,3,2]diazaborinin-4-ium-5-uide (HPIB1). To a solution of **5a** (2131 mg, 4 mmol) in dry dichloromethane (50.0 mL) and THF (10 ml), a solution of an equivalent amount of 2,3-dichloro-5,6-dicyanobenzoquinone (908 mg; 1 eq.) dissolved in benzene was added dropwise over an hour and the reaction mixture stirred for an additional 3 hours. After the completion of the reaction, the resulting reaction mixture was dried under reduced pressure using a rotatory evaporator. The crude product was dissolved in a minimum amount of dichloromethane (DCM) and filtered to remove any solid impurities. The filtrate was treated with triethylamine (3.0 mL) followed by $BF_3{\cdot}Et_2O$ (3.0 mL) and the reaction mixture allowed to stir for 30 minutes at room temperature. It was then subjected to dryness under reduced pressure and the crude product thus obtained was purified by silica gel column chromatography (DCM/hexane 40 : 60) to obtain the desired product as an orange-red solid. Yield: 13% (301 mg). Anal. calcd for $C_{36}H_{25}BF_2N_4O$: C, 74.75; H, 4.36; N, 9.69. Found: C, 74.35; H, 4.40; N, 9.63. **^{1}H NMR** (500 MHz, $CDCl_3$) δ = 7.92 (s, 2H), 7.49–7.45 (m, 5H), 7.29–7.15 (m, 12H), 6.93 (d, J = 3 Hz, 2H), 6.59 (s, 1H), 6.50 (s, 2H). **^{13}C NMR** (125 MHz, $CDCl_3$) δ = 155.09, 144.47, 143.03, 142.72, 136.42, 135.41, 135.33, 132.18, 131.32, 131.23, 131.15, 130.81, 130.07, 129.94, 129.10, 128.84, 128.62, 128.48, 128.35, 127.43, 127.04, 126.85, 123.52, 122.12, 118.41, 114.56 ppm. **^{11}B NMR** (160.4 MHz, $CDCl_3$) δ = −0.661 (t, 1B) ppm; **^{19}F NMR** (470.6 MHz, $CDCl_3$): δ = −143.42 (dq, 1F), −146.68 (dq, 1F) ppm; **IR** (KBr pellet): 3445, 3107, 2925, 2485, 1590, 1557, 1493, 1455, 1412, 1381, 1387, 1272, 1259, 1225, 1181, 1147, 1131, 1113, 1075, 1052, 942, 767, 734, 709, 671, 584, 552, 408 cm^{-1}; **HRMS** (ESI): m/z calcd for $C_{36}H_{25}BF_2N_4O$ $[M + Na]^+$: 601.2; found: 601.1.

Preparation of 10-(5-chloro-2-hydroxy-3-(1,4,5-triphenyl-1*H*-imidazol-2-yl)phenyl)–5,5-difluoro-5*H*-dipyrrolo[1,2-c:2′,1′-f][1,3,2] diazaborinin-4-ium-5-uide (HPIB2). HPIB2 was prepared fol-

lowing the above procedure described for **HPIB1** using **5b** (2268 mg, 4 mmol) in place of **5a**. Yield: 15.50% (380 mg). Anal. calcd for $C_{36}H_{24}BClF_2N_4O$: C, 70.55; H, 3.95; N, 9.14. Found: C, 70.31; H, 4.02; N, 9.11. **^{1}H NMR** (500 MHz, $CDCl_3$) δ = 7.89 (s, 2H), 7.63–7.57 (m, 3H), 7.44 (d, J = 7.5 Hz, 2H), 7.37–7.23 (m, 7H), 7.16 (t, J = 7 Hz, 2H), 6.94 (d, J = 7 Hz, 4H), 6.49 (d, J = 2.5 Hz, 3H). **^{13}C NMR** (125 MHz, $CDCl_3$) δ = 152.88, 144.60, 141.15, 139.30, 135.35, 134.38, 134.19, 133.19, 132.93, 131.46, 131.20, 130.98, 130.76, 130.21, 129.38, 129.16, 128.59, 128.20, 127.94, 127.63, 126.27, 125.99, 123.46, 118.52, 112.09 ppm. **^{11}B NMR** (160.4 MHz, $CDCl_3$) δ = −0.709 (t, 1B) ppm; **^{19}F NMR** (470.6 MHz, $CDCl_3$): δ = −141.93 (dq, 1F), −147.86 (dq, 1F) ppm; **IR** (KBr pellet): 3420, 3107, 2924, 2884, 1563, 1560, 1505, 1445, 1412, 1389, 1260, 1228, 1113, 1079, 1045, 1010, 950, 924, 871, 772, 997, 552, 417 cm^{-1}; **HRMS** (ESI): m/z calcd for $C_{36}H_{24}BClF_2N_4O$ $[M + H]^+$: 613.2; found: 613.2.

Preparation of 10-(5-chloro-3-(4,5-diphenyl-1-(*p*-tolyl)-1*H*-imidazol-2-yl)-2-hydroxy-phenyl)-5,5-difluoro-5*H*-dipyrrolo [1,2-c:2′,1′-f][1,3,2]diazaborinin-4-ium-5-uide (HPIB3). **HPIB3** was prepared following the above procedure described for **HPIB1** using **5c** (2325 mg, 4 mmol) in place of **5a**. Yield: 16.63% (417 mg). Anal. calcd for $C_{37}H_{26}BClF_2N_4O$: C, 70.89; H, 4.18; N, 8.94. Found: C, 70.85; H, 4.21; N, 8.93. **^{1}H NMR** (500 MHz, $CDCl_3$) δ = 7.92 (s, 2H), 7.47–7.44 (m, 2H), 7.31–7.26 (m, 5H) 7.21–7.13 (m, 8H), 7.94 (d, J = 5 Hz, 2H), 6.64 (d, J = 2.5 Hz, 1H), 6.51 (d, J = 4 Hz, 2H), 2.43 (s, 3H). **^{13}C NMR** (125 MHz, $CDCl_3$) δ = 155.11, 144.44, 143.13, 142.81, 140.18, 135.44, 135.24, 133.76, 132.27, 131.39, 131.25, 131.17, 130.74, 130.64, 129.25, 128.77, 128.60, 128.33, 128.16, 127.37, 127.07, 126.86, 123.48, 122.10, 118.41, 114.68, 21.30 ppm. **^{11}B NMR** (160.4 MHz, $CDCl_3$) δ = −0.709 (t, 1B) ppm; **^{19}F NMR** (470.6 MHz, $CDCl_3$): δ = −141.93 (dq, 1F), −147.89 (dq, 1F) ppm; **IR** (KBr pellet): 3435, 2925, 2851, 1558, 1516, 1412, 1388, 1299, 1258, 1144, 1108, 1077, 1042, 1009, 916, 916, 874, 787, 741, 704, 548, 412 cm^{-1}; **HRMS** (ESI): m/z calcd for $C_{37}H_{26}BClF_2N_4O$ $[M + H]^+$: 627.2; found: 627.2.

Preparation of 10-(5-chloro-3-(1-(4-chlorophenyl)-4,5-diphenyl-1*H*-imidazol-2-yl)-2-hydroxy-phenyl)-5,5-difluoro-5*H*-dipyrrolo [1,2-c:2′,1′-f][1,3,2]diazaborinin-4-ium-5-uide (HPIB4). **HPIB4** was prepared following the above procedure described for **HPIB1** using **5d** (2406 mg, 4 mmol] in place of **5a**. Yield: 15% (389 mg). Anal. calcd for $C_{36}H_{23}BCl_2F_2N_4O$: C, 66.80; H, 3.58; N, 8.66. Found: C, 66.57; H, 3.61; N, 8.55. **^{1}H NMR** (500 MHz, $CDCl_3$) δ = 7.93 (s, 2H), 7.47–7.45 (m, 4H), 7.35–7.26 (m, 3H) 7.22 (m, 6H), 7.15 (d, J = 7.5 Hz, 2H), 6.90 (s, 2H), 6.71 (s, 1H), 6.51 (d, J = 3 Hz, 2H). **^{13}C NMR** (125 MHz, $CDCl_3$) δ = 154.89, 144.56, 142.89, 142.37, 136.07, 135.37, 134.77, 131.26, 131.20, 131.10, 130.31, 129.70, 129.16, 128.86, 128.65, 128.42, 127.69, 127.24, 126.93, 123.92, 122.48, 118.49, 114.33. **^{11}B NMR** (160.4 MHz, $CDCl_3$) δ = −0.681 (t, 1B) ppm; **^{19}F NMR** (470.6 MHz, $CDCl_3$): δ = −143.62 (dq, 1F), −146.51 (dq, 1F) ppm; **IR** (KBr pellet): 3407, 2924, 2856, 2884, 1602, 1590, 1560, 1537, 1493, 1458, 1412, 1387, 1353, 1260, 1181, 1107, 1074, 988, 942, 980 cm^{-1}; **HRMS** (ESI): m/z calcd for $C_{36}H_{23}BCl_2F_2N_4O$ $[M + H]^+$: 647.1; found: 647.1.

Results and discussion

Synthesis and characterization

A simple synthetic route adopted for preparation of **HPIB1–HPIB6** is shown in Scheme 1. Compounds **3a–3d** were obtained by the reaction of the respective salicylaldehyde derivatives [R_1 = H (**1a**), Cl (**1b**)] and phenylamine counterparts [R_2 = H (**2a**), CH_3 (**2b**), Cl (**2c**)] with benzyl in the presence of ammonium acetate following literature procedures.[19]

Formylation of **3a–3d** following the Duff reaction gave **4a–4d** with free formyl groups.[20] The aldehydes **4a–4d** reacted

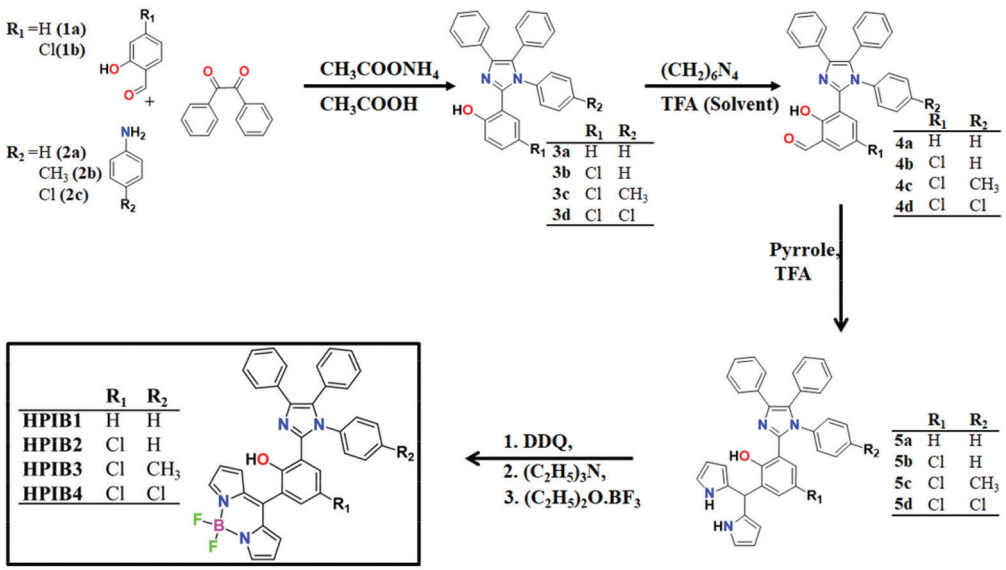

Scheme 1 The synthetic procedure adopted for HPIB1–HPIB4.

with an excess of pyrrole in the presence of catalytic amounts of trifluoroacetic acid to afford dipyrromethane derivatives **5a–5d**.[21] Ultimately, boron dipyrromethene derivatives **HPIB1–HPIB4** were prepared by oxidation of the respective dipyrromethanes **5a–5d** with 2,3-dichloro-5,6-dicyano-benzoquinone (DDQ) followed by addition of triethylamine (Et_3N) and $BF_3{\cdot}Et_2O$ successively.[22] The compounds (**HPIB1–HPIB4**) were thoroughly characterized by elemental analyses, IR, ESI-MS and NMR ($^1H/^{13}C/^{11}B/^{19}F$) studies (see ESI†). The molecular structures of **HPIB1–HPIB4** have also been unequivocally determined by X-ray single crystal analyses. The compounds under investigation showed good solubility in dichloromethane (DCM), chloroform, dimethyl sulfoxide (DMSO), dimethylformamide (DMF) and acetonitrile, however, poor solubility in methanol, ethanol, hexane, toluene, benzene and water.

Absorption and emission spectroscopy

The electronic absorption spectra of **HPIB1–HPIB4** (DMF) displayed sharp absorption at ~505 nm [$\lambda_{abs,max}$ = 505; **HPIB1**, 507; **HPIB2**, 506; **HPIB3**, and 505 nm; **HPIB4**] along with a shoulder at 480 nm owing to 0–0 and 0–1 vibrational bands of S0–S1 transition in the BODIPY core (Fig. 1 and Fig. S21†). Also, these compounds displayed a weak band at ~340–350 nm due to the *meso*-phenyl-BODIPY core assignable to S0–S2 transitions.[22a] The absorption bands are in good agreement with reported values for phenyl BODIPY systems.[22a] Their emission spectra (DMF) showed a single emission band at ~535 nm [$\lambda_{em,max}$ = **HPIB1**, 536; **HPIB2**, 535; **HPIB3**, 535; and **HPIB4**, 536 nm] (Fig. 1 and Fig. S22†).

It has been observed that the emission maxima of these compounds lie at almost the same position; however, the emission intensities of **HPIB2** and **HPIB3** are high relative to **HPIB1** and **HPIB4**. The lower fluorescence intensities of **HPIB1** and **HPIB4** may be attributed to the more active intramolecular rotations in these systems. In addition, fluorescence excitation spectra at the respective emission maxima of these compounds resemble the absorption spectra, except for a small red-shift (Fig. S23†). Small mismatch of the excitation spectra may probably arise due to conformational isomerization owing to intramolecular rotations (Fig. S23†).[23] Absorption and emission spectra have also been acquired by varying the concentration of the compounds. Emission intensity gradually enhanced with increasing concentrations of the compounds up to 50 μM and thereafter it diminished (Fig. S28–S31†). In addition, emission maxima displayed continual red-shift with increasing concentrations (up to 25–30 nm on going from 10 μM to 150 μM). The observed fluorescence quenching may be due to short-range intermolecular interactions as well as active intramolecular rotation/molecular flexibility.[22b] The red-shift of the emission maxima clearly indicated short-range intermolecular interactions.[22b] However, the intensity of absorption maxima augmented with increasing concentration without any shifts in their positions (Fig. S24–S27†).

The absorption and emission spectra of these compounds have also been acquired in various solvents (Fig. 2 and Fig. S32–S34†). The examination of the emission spectra revealed that the intensity of the bands in non-polar solvents is high relative to polar solvents (Fig. 2 and Fig. S32–S34†). High emission intensity in non-polar solvents may be related to strong intramolecular H-bonding inducing rigidity in the system. On the other hand, low emission intensity may be ascribed to intermolecular H-bonding and/or other interactions with solvent molecules allowing the system to lose energy non-radiatively and making it less fluorescent.

Furthermore, the emission spectra of the compounds in solvents like toluene and benzene showed intense and slightly red-shifted maxima relative to other solvents. This is in contrast to the usual blue-shifted emission in non-polar solvents like benzene and toluene. Most probably this may be due to aggregation as these solvents can serve as non-solvents (poor solvents) for the aggregation process.[24] A quantitative idea about the emission behaviour of **HPIB1–HPIB4** in various solvents has further been deduced from fluorescence quantum yields (Table S1†). Notably, the absorption spectra did not show any appreciable changes with the polarity of the solvent and the absorption maxima appeared at almost the same position as in DMF (Fig. S35–S38†).

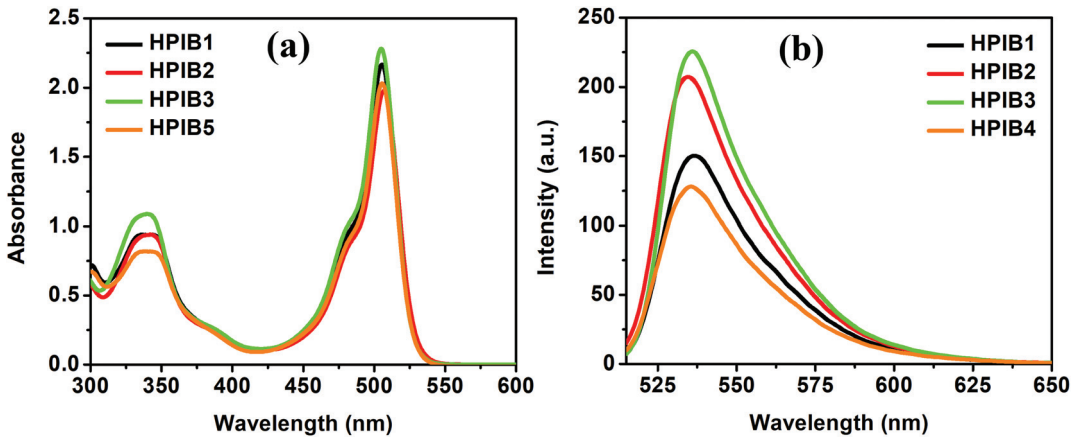

Fig. 1 Absorption (a) and emission spectra (b) of **HPIB1–HPIB4** in DMF (*c*; 50 μM, DMF, λ_{ex}; 505 nm).

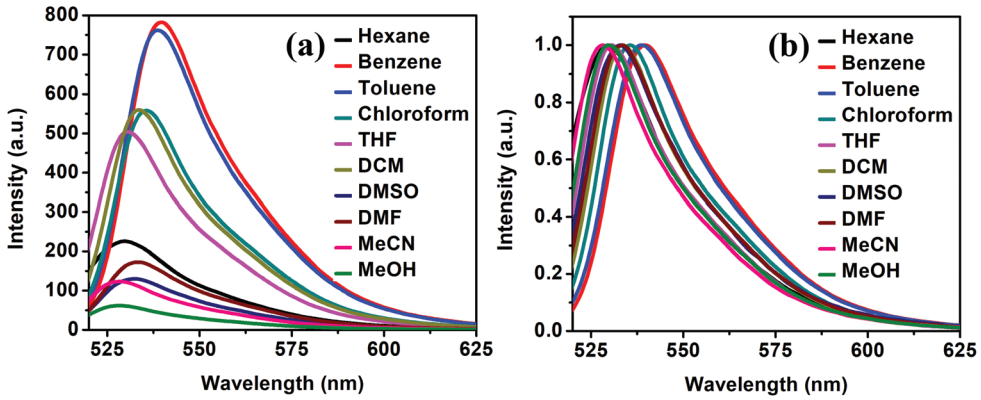

Fig. 2 Emission spectra (a) of **HPIB2** and its normalized representation (b) in different solvents with varying polarities (*c*; 50 μM, λ_{ex}; 505 nm); [THF = tetrahydrofuran, DCM = dichloromethane, DMSO = dimethyl sulfoxide, DMF = *N*,*N*-dimethylformamide, MeCN = acetonitrile, MeOH = methanol].

Aggregation-induced emission

The aggregation-induced emission behaviour of **HPIB1–HPIB4** has been investigated by acquiring the absorption spectra of these compounds in DMF/water mixtures with varying water content (f_w). As depicted in Fig. 3 and S39–S41,† the absorption spectra did not show any appreciable changes with increasing f_w (up to 50%). However, at an f_w of 60% they showed broadening of the bands and lowering of the absorption intensity. A further increase of the water fraction led to an incessant decrease of intensity with an appreciable red-shift, and ultimately at an f_w of 99% the intensity significantly went down and the absorption band radically broadened. Such a change in the intensity of the band and broadening may be related to the aggregation process[25] and may arise due to Mie scattering. In fact, the aggregation process leads to transparent nanoparticle suspensions which scatter light and cause the broadening of the absorption bands with an apparent red-shift (level-off tails).[25] Moreover, the red-shift of the absorption maxima at high water fractions (f_w > 50%) suggested J-aggregation.[25b]

Emission spectra have also been acquired in the same solvent system. As shown in Fig. 4 and Fig. S42,† emission intensity enhanced with increasing f_w without any change in the position of the emission maxima (λ_{em} = ~535 nm) up to an f_w of 50%. An increase of f_w to 60% led to small red-shifted emission with higher emission intensity relative to that in DMF along with a new band at ~615 nm. A further increase of f_w (>60%) led to apparent dual emission at ~560 and ~610 nm compared to emission maxima at ~535 nm (in pure DMF). The emission behavior at a high water fraction may be attributed to AIE.[3] Furthermore, emission behavior has also been investigated by estimation of fluorescence quantum yields (Φ_f) at various water fractions (f_w: 0% and 60%–99%). Calculated Φ_f are high at higher water fractions (f_w: >50%) relative to those in DMF (f_w: 0%) for the respective compounds (Table 1). This clearly indicated the occurrence of AIE for all these derivatives at high f_w (Table 1). High emission intensity for **HPIB1–HPIB4** in the aggregated state (f_w: >50%) has also been supported by time-resolved fluorescence studies. The time-resolved emission spectra were acquired in DMF/water mixtures with varying

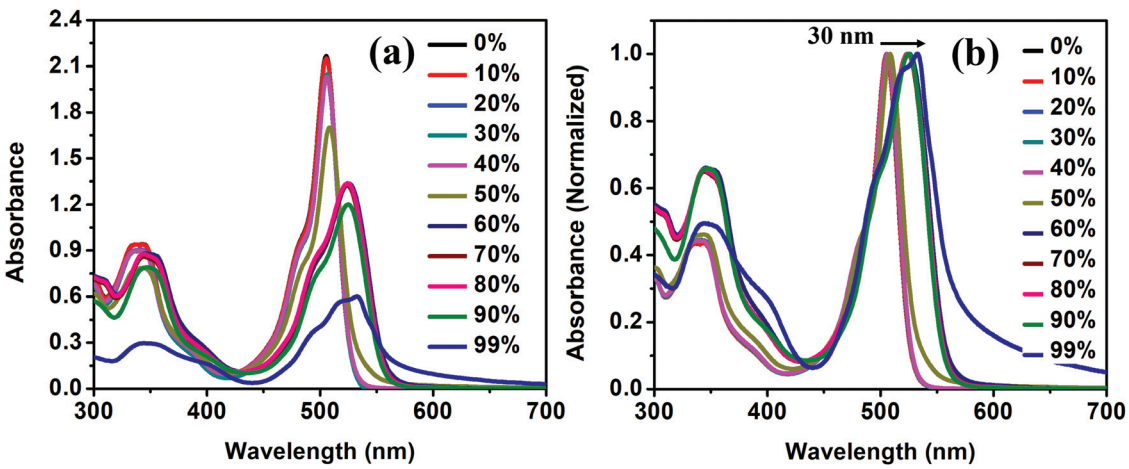

Fig. 3 Absorption spectra (a) of **HPIB1** and its normalized representation (b) in DMF/water mixtures with increasing water volume fractions (*c*; 50 μM).

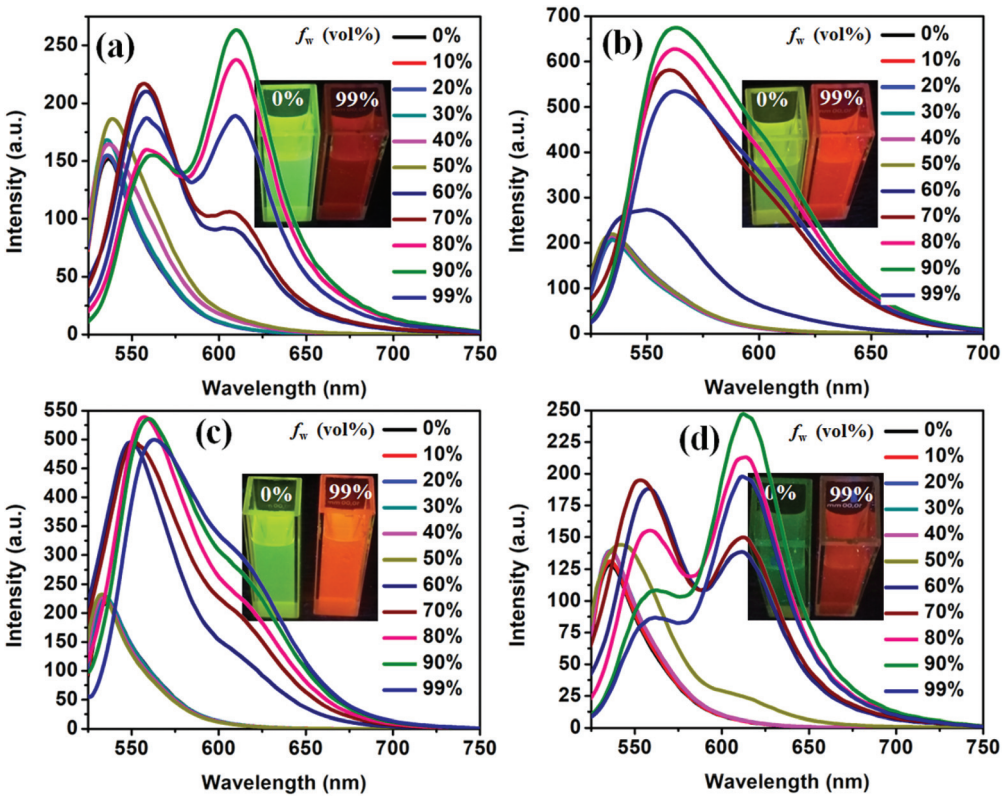

Fig. 4 Emission spectra of **HPIB1** (a), **HPIB2** (b), **HPIB3** (c) and **HPIB4** (d) in DMF/water mixtures with increasing water volume fractions (*c*; 50 μM, λ_{ex}; 505 nm).

Table 1 Fluorescence lifetimes (τ_f)[a] and quantum yields (Φ_f)[b] at varying f_w for **HPIB1–HPIB4**

	HPIB1		HPIB2		HPIB3		HPIB3	
Water content (f_w)	τ_f/ns	Φ_f	τ_f/ns	Φ_f	τ_f/ns	Φ_f	τ_f/ns	Φ_f
0%	1.07	0.039	1.21	0.053	1.17	0.059	1.04	0.033
60%	1.87	0.077	2.57	0.059	2.49	0.197	2.55	0.057
70%	1.91	0.081	3.85	0.210	2.50	0.219	2.67	0.059
80%	2.34	0.099	3.96	0.207	2.67	0.223	2.73	0.071
90%	2.53	0.110	4.17	0.240	3.57	0.229	2.96	0.074
99%	2.52	0.107	3.89	0.200	3.37	0.216	2.85	0.070

[a] The average lifetime is given; ns = nanosecond; the excitation wavelength is 482 nm. [b] Fluorescence quantum yields were determined using the rhodamine 6G dye (H_2O, λ_{ex} = 530 nm, λ_{em} = 552 nm, Φ_f = 0.95) as the standard; stock solutions of **HPIB1–HPIB4** were prepared in DMF.

water fraction (f_w: 0% and 60%–99%) and best fitted to a bi-exponential model as depicted in Table 1 and Fig. S43.† The observed lifetimes in the aggregated state (f_w: >50%) are high relative to those in DMF (f_w: 0%) for all these derivatives and are in good agreement with available data on AIE luminogens.[25] Hence, the high fluorescence lifetime may be related to the aggregation-induced emission behavior of these compounds.[25]

Overall, data obtained from the absorption and emission spectra as well as measured fluorescence lifetimes and quantum yields suggested AIE behavior for these compounds. These compounds displayed dual emission in the range of 500–700 nm in the aggregated state and among these **HPIB1** and **HPIB4** exhibited prominent emission at ~616 nm with a shoulder at ~560 nm; however, **HPIB2** and **HPIB3** showed prominent emission at ~560 nm with a shoulder at ~610 nm. Furthermore, **HPIB2** and **HPIB3** displayed high emission intensity with a relatively small red-shift in the aggregated state, while **HPIB1** and **HPIB4** showed relatively weak emission with large red-shifted maxima (Fig. 4). The anomalies in the emission behavior of these compounds may be related to the orientation of the respective compounds causing distinct molecular packing in the aggregated state which has been explained (*vide-infra*) on the basis of crystal structures.

Aggregate morphology and size

The effects of variation of substituents on aggregation behavior and their co-relation with optical responses have been examined by subjecting the aggregates (DMF/water mixture; f_w, 99%) to field emission scanning electron microscopy (FESEM) (Fig. 5). The FESEM images revealed that each of these compounds (**HPIB1–HPIB4**) exhibit different aggregate morphology which has been related to the changes in packing arrangement of molecules due to variation of the substituents. As shown in Fig. 5, **HPIB1** gave Thuja leaf shaped nanoclusters, while **HPIB2** rope-like fibrous nanoclusters. On the other hand, **HPIB3** and **HPIB4** gave nano-sphere aggregates. Thus, it can be concluded that the nano-aggregates of these derivatives display unique morphologies which strongly depend on the substituents under analogous conditions. This confirmed the distinct emission behavior of these compounds. Furthermore, the size of the aggregate has been determined by dynamic light scattering (DLS) studies under analogous conditions (at an f_w of 99%) and it lies in the range of 89 nm to 462 nm [89 nm, **HPIB1**; 462 nm, **HPIB2**; 341 nm, **HPIB3**; and 178 nm; **HPIB4**] (Fig. S44†).

Restricted intramolecular rotations (RIRs) and viscochromism

The compounds presented in this study have been designed in such a way that they can serve as FMRs wherein four bulky phenyl rings are present around the imidazole moiety along with the BODIPY core connected through a single bond. In such systems, the rotations of the constituent units are active in low-viscous medium/dilute solution promoting the non-radiative decay process and thereby weakening the fluorescence intensity. On the other hand, intra-molecular rotations get restricted in viscous medium populating the radiative channels causing large emission enhancements.[3,13a,25]

The restricted intramolecular rotations (RIRs) and the possible role of these fluorophores as FMRs have been assessed by viscosity-dependent absorption and emission spectral studies in methanol/glycerol mixtures by varying the viscosity of the medium from 0.61 (CH_3OH; f_g 0%) to 793.0 cP (f_g 90%).[26] Absorption spectra did not show any significant changes in the intensity and position of the absorption maxima (Fig. S45†). However, with an increase in viscosity from 0.6 to 793 cP, the emission intensity enhanced appreciably (30; **HPIB1**, 25; **HPIB2**, 16; **HPIB3** and 25-fold; **HPIB4**) without changes in the position of emission maxima at ~532 nm [532; **HPIB1**, 532; **HPIB2**, 534; **HPIB3** and 534 nm; **HPIB4**] (Fig. 6a and Fig. S46a–S48a†). The time-resolved emission decay profiles of these derivatives at varying viscosities revealed the gradual increase of the fluorescence lifetime (τ_f) with increasing viscosity of the medium as depicted in Fig. 6b, Fig. S46b–S48b and Table S2.† Also, fluorescence quantum yields (Φ_f) appreciably enhanced from ~1% [0.9%; **HPIB1**, 1.2%; **HPIB2**, 1.5%; **HPIB3**, and 1.2%; **HPIB4**] at a viscosity of 0.6 cP in methanol to ~70% [67%; **HPIB1**, 69.7%; **HPIB2**, 67.3%; **HPIB3** and 69.3%; **HPIB4**] at 793 cP in 90% glycerol fractions (Table S3†). Hence, it may be concluded that these derivatives are sensitive toward the viscosity of the medium and these observations are consistent with earlier reports.[13,26]

Furthermore, radiative (k_r) and non-radiative (k_{nr}) rate constants calculated using measured Φ_f and τ_f revealed that k_r remains almost constant (0.06–0.15 ns^{-1}) at various viscosities of the medium under investigation (Table S4†). On the other hand, k_{nr} sharply decreases (0.90 to 0.07) with increasing viscosity of the medium (Table S4†). The decrease in k_{nr} values clearly confirmed that significant enhancement in quantum efficiency and the average lifetime at higher viscosity is due to

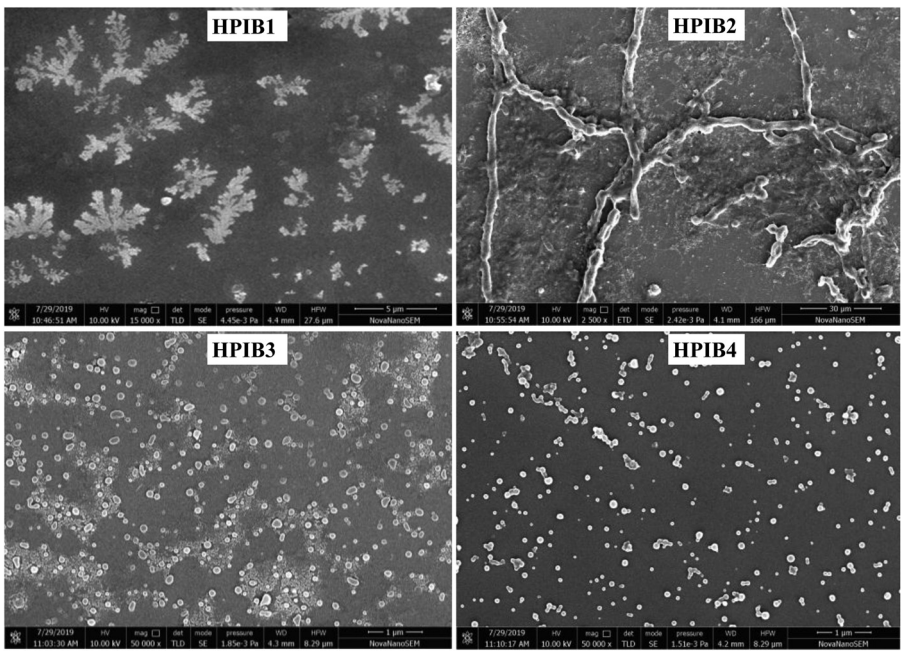

Fig. 5 The FESEM image of the nano-aggregates of **HPIB1–HPIB4** formed in DMF/water mixtures at an f_w of 99% (c; 50 μM).

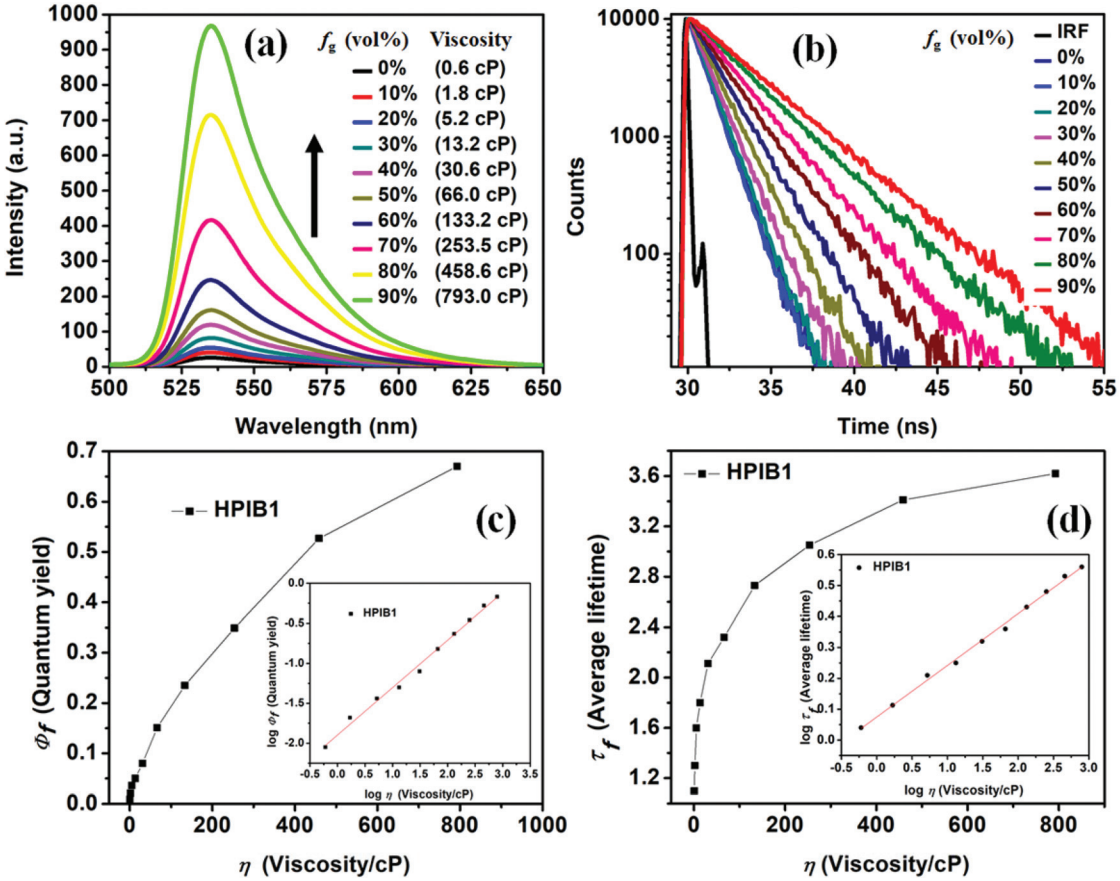

Fig. 6 (a and b) Emission spectra (c; 50 μM, λ_{ex}; 505 nm) (a) and time-resolved fluorescence decay profiles (b) (λ_{ex} = 482 nm and λ_{em} = ~535 nm), at different viscosities of the medium (in methanol/glycerol mixtures); (c) a plot of fluorescence quantum yield (Φ_f) as a function of viscosity; the inset shows the linearity in the entire range of viscosity under investigation obtained in the log plot; (d) a plot of the fluorescence lifetime (τ_f) as a function of viscosity; the inset shows the linearity in the entire range of viscosity under investigation obtained in the log plot according to the Förster–Hoffmann equation for **HPIB1**.

the suppression of non-radiative decay processes with increasing viscosity of the medium and the observations are in accord with the Förster–Hoffmann theory.[13c,26,27] Furthermore, a plot of fluorescence quantum yields (Φ_f)/lifetimes (τ_f) *vs.* viscosity (η) has been obtained following the Förster–Hoffmann equations (Fig. 6 and Fig. S46–S48†).[26,27]

$$\log(\Phi_f) = C + x\log(\eta) \quad (1)$$

$$\log(\tau_f) = C' + y\log(\eta) \quad (2)$$

where C/C' and x/y represent constants.

As expected, a plot of $\log \Phi_f$ *vs.* $\log \eta$ showed a straight line with a slope of 0.593 (**HPIB1**), 0.560 (**HPIB2**), 0.550 (**HPIB3**) and 0.581 (**HPIB4**), respectively. These are consistent with earlier reports on BODIPY based FMRs (Fig. 6c and Fig. S46c–S48c†).[26,27] Furthermore, a similar observation has also been made from a plot between $\log \tau_f$ and $\log \eta$, which showed a slope of 0.167 (**HPIB1**), 0.190 (**HPIB2**), 0.176 (**HPIB3**), and 0.133 (**HPIB4**). Notably, these are also analogous to the typical slopes (0.2–1.4) obtained in earlier reports (Fig. 6d and Fig. 46d–S48d†).[27] Thus, it is concluded that these compounds serve as FMRs in various media including biological systems.

Crystal structures, packing diagrams and the mechanism of AIE

In order to gain deep insight into AIE behavior and its relationship with molecular packing, the structures of **HPIB1–HPIB4** have been determined by X-ray single crystal analyses (Fig. 7). Suitable single crystals for these compounds were grown by slow evaporation of DCM/methanol solution. The crystal data and refinement parameters are summarized in Table 3 and Tables S5–S7 in the ESI.†

Careful examination of the dihedral angles (Table 2) revealed highly twisted and non-planar orientations for these derivatives. The phenol (ring A) and imidazole rings are almost co-planar as evidenced by small dihedral angles (3.08°; **HPIB1**, 6.34°; **HPIB2**, 12.86°; **HPIB3** and 3.13°; **HPIB4**) due to intramolecular H-bonding. The intramolecular H-bond distances (–O1–H···N3) are small and fall in the range of 1.711–1.770 Å [1.766; **HPIB1**, 1.711; **HPIB2**, 1.770; **HPIB3**, and 1.759 Å; **HPIB4**], while –O1–H···N3 angles are in range of

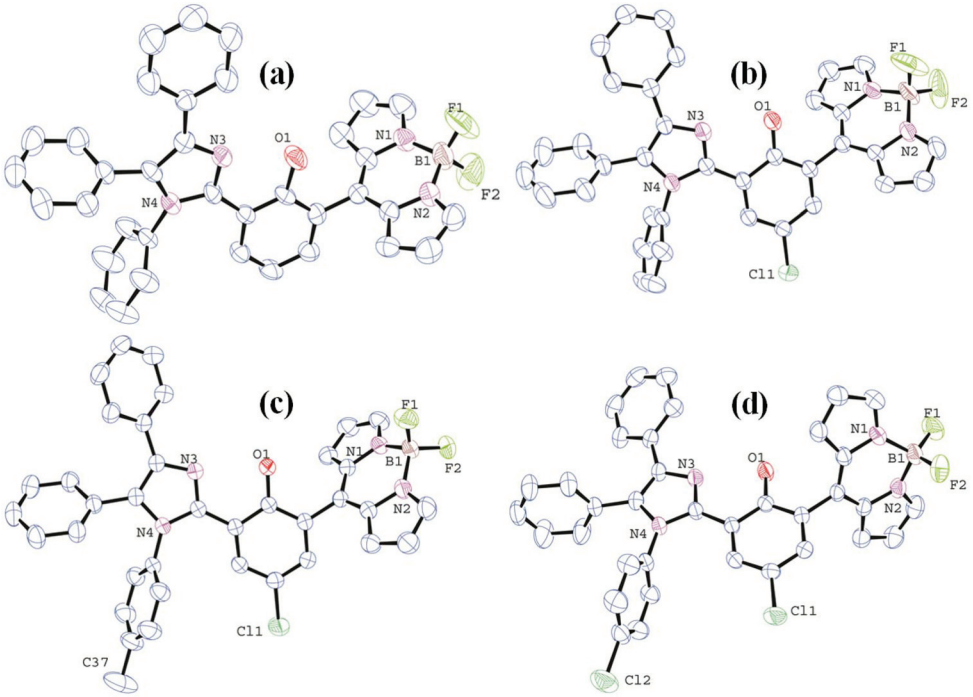

Fig. 7 ORTEP views of (a) **HPIB1**, (b) **HPIB2**, (c) **HPIB3** and (d) **HPIB4** at 50% ellipsoid probability (hydrogen atoms have been omitted for clarity).

Table 2 Dihedral angles between phenyl and imidazole rings as well as the phenyl ring and the BODIPY core, extracted from single crystal XRD data for **HPIB1–HPIB4**

	HPIB1	HPIB2	HPIB3	HPIB4
Between the BODIPY core and phenyl ring **A**	80.93°	61.85°	60.68°	71.22°
Between the imidazole ring and phenyl ring **A**	3.08°	6.34°	12.86°	3.13°
Between the imidazole ring and phenyl ring **B**	86.68°	83.83°	73.94°	87.05°
Between the imidazole ring and phenyl ring **C**	76.34°	72.21°	50.57°	78.27°
Between the imidazole ring and phenyl ring **D**	3.39°	3.34°	32.16°	23.21°

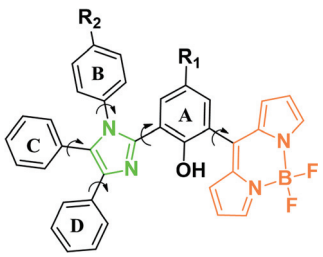

140.94–148.98° [148.45°; **HPIB1**, 140.94°; **HPIB2**, 149.62°; **HPIB3**, and 148.98°; **HPIB4**]. The observed parameters clearly revealed strong intramolecular H-bonding and offered necessary co-planarity between two units (phenol and imidazole rings) for these derivatives.[28] Moreover, these derivatives showed distinct dihedral angles for each ring probably due to substituent variation and their electronic and steric effects (Table 2).

Furthermore, the twisted and non-planar orientation enables the system to avoid detrimental π–π stacking that creates excimers/exciplexes responsible for ACQ.[29] In fact, the crystal structures of **HPIB1–HPIB4** completely lack detrimental π–π stacking. Instead, these exhibited C–H···π, B–F···H–C and B–F···π interactions favoring J-type packing responsible for emission enhancement in the aggregated state with an appreciable red-shift.[8] Also, these interactions interlock molecules and provide physical restraints on intramolecular rotations in aggregated/dense medium and, consequently, emission is enhanced.

The crystal structures of **HPIB1** and **HPIB2** involve C–H···π and B–F···H–C interactions and yield J-type aggregates. In **HPIB1**, C–H···π (2.817 Å) forms long ordered J-type packing which is further linked by B–F···H–C (2.348 Å) to create a 2D network (Fig. S49†). **HPIB2** showed J-type packing due to both C–H···π (2.663 Å) and B–F···H–C (2.571 Å) interactions (Fig. 8 and Fig. S50†). On the other hand, the crystal structure of **HPIB3** involves B–F···H–C (2.511 Å) and B–F···π (3.120 Å) interactions instead of C–H···π interactions to form J-clusters (Fig. 9 and Fig. S51†). Furthermore, **HPIB4** involves C–H···π (2.755 Å) and B–F···π (3.143 Å) interactions and displays J-type packing similar to other derivatives (Fig. 10 and Fig. S52†).

Thus it is concluded that J-type packing in the aggregated state is responsible for emission enhancement (*i.e.* AIE) in addition to the RIR in these systems. From the crystal structures, it can be seen that each derivative exhibits a distinct site of interaction between molecules and leads to a different packing pattern and, accordingly, they exhibited diverse emis-

Table 3 Selected crystallographic parameters for **HPIB1–HPIB4**

Crystal data	**HPIB1**	**HPIB2**	**HPIB3**	**HPIB4**
Empirical formula	$C_{36}H_{25}BF_2N_4O$	$C_{36}H_{24}BClF_2N_4O$	$C_{37}H_{26}BClF_2N_4O$	$C_{36}H_{23}BCl_2F_2N_4O$
Crystal system	Triclinic	Monoclinic	Monoclinic	Triclinic
Space group	$P\bar{1}$	$P2_1/n$	$P2_1/c$	$P\bar{1}$
a (Å)	10.208(2)	9.6016(3)	9.1437(2)	9.5668(7)
b (Å)	10.769(2)	25.7083(6)	14.2235(3)	13.2433(9)
c (Å)	14.485(3)	12.6994(3)	24.9508(5)	13.9708(9)
α (°)	111.348(5)	90	90	104.534(2)
β (°)	90.210(5)	105.329(3)	97.853(2)	103.397(2)
γ (°)	97.478(5)	90	90	104.401(2)
V (Å^3)	1468.3(5)	3023.21(1)	3214.55(1)	1575.80(2
Z	2	4	4	2
F (000)	598.0	1264	1296	664
ρ_{calc} (g cm^{-3})	1.306	1.346	1.295	1.364
T (K)	273(2)	150(2)	150(2)	273(2)
μ (mm^{-1})	0.088	0.176	0.167	0.254
Reflns collected	32 481	26 415	47 535	38 778
GOF on F^2	1.008	1.017	1.026	1.007
Final R_1	0.1069	0.0602	0.0576	0.0485
Final wR_2	0.1635	0.1602	0.1463	0.1084

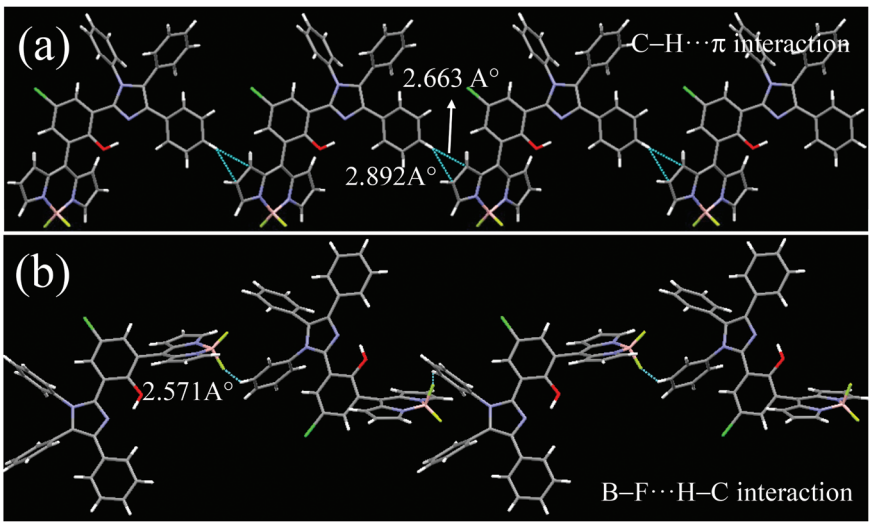

Fig. 8 (a and b) J-type packing *via* C–H···π and B–F···H–C interactions respectively extracted from single crystal XRD data for **HPIB2**.

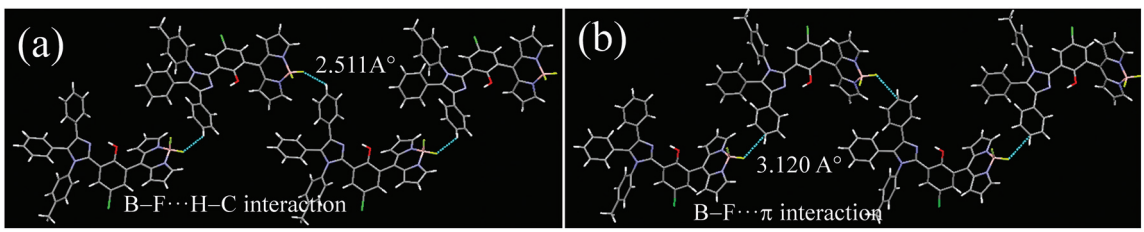

Fig. 9 (a and b) J-type packing due to B–F···H–C and B–F···π interactions extracted from single crystal XRD data for **HPIB3**.

sions. Furthermore, the extent of emission enhancement and red shift can be rationalized on the basis of twisting of structural entities. Usually systems exhibiting twisting to a greater extent display red-shifted emission to a greater extent with low intensity owing to loss of excitation energy in non-radiative pathways.[29] It can be seen from the dihedral angles (Table 2) of these derivatives that **HPIB1** and **HPIB4** are relatively more twisted and have greater dihedral angles. In contrast to **HPIB1**

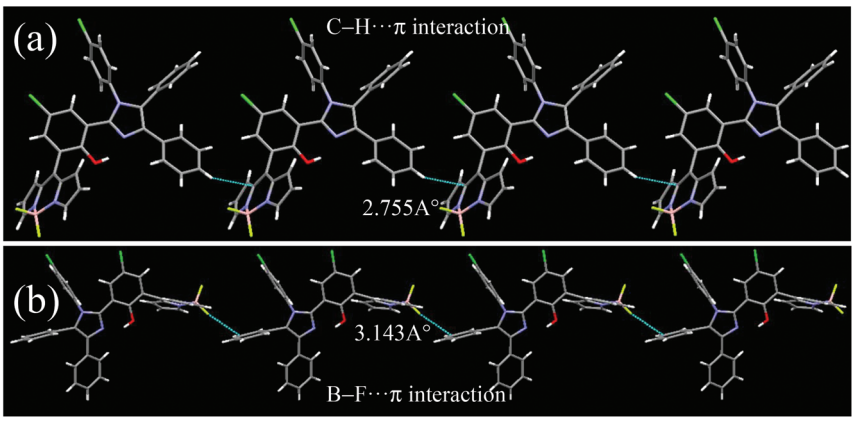

Fig. 10 (a and b) J-type packing structures due to C–H···π and B–F···π interactions respectively extracted from single crystal XRD data for **HPIB4**.

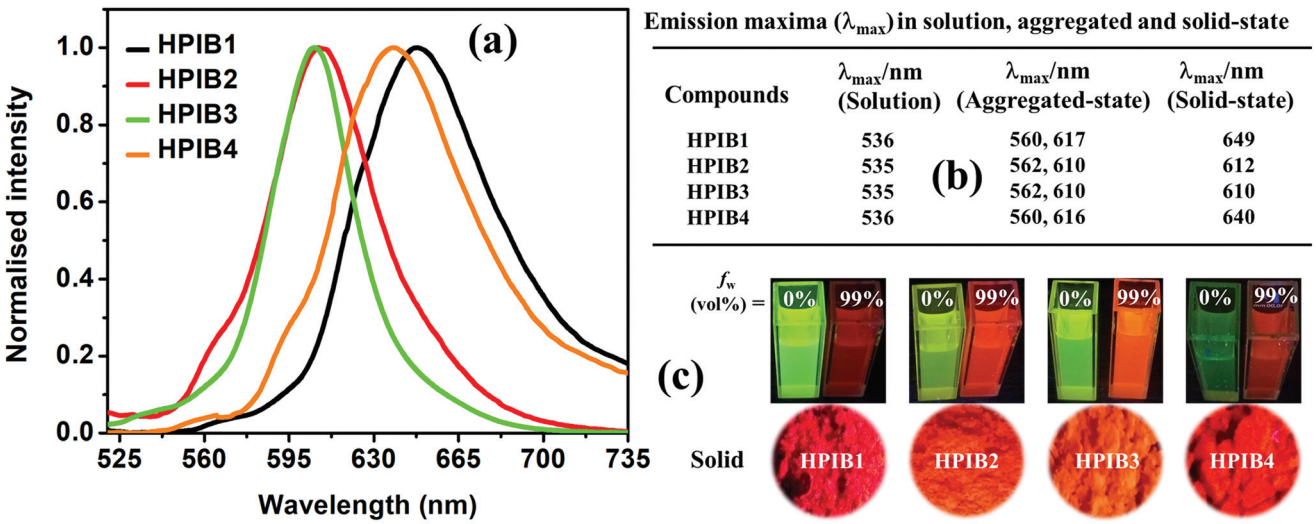

Compounds	λ_{max}/nm (Solution)	λ_{max}/nm (Aggregated-state)	λ_{max}/nm (Solid-state)
HPIB1	536	560, 617	649
HPIB2	535	562, 610	612
HPIB3	535	562, 610	610
HPIB4	536	560, 616	640

Fig. 11 (a) Emission spectra in the solid state (powder, λ_{ex} = ~505 nm); (b) a summary of emission maxima in solution, aggregated and solid states; and (c) photographs of **HPIB1–HPIB4** under UV irradiation (λ_{ex}, 365 nm) for solution (f_w of 0%), aggregated (f_w of 99%) and solid states (powder).

and **HPIB4**, for **HPIB2** and **HPIB3** the dihedral angles are small between BODIPY and the phenyl ring (ring A) as well as for other rings, and therefore these compounds displayed strong emission with a small red-shift.

Solid state emission

As shown in Fig. 11, **HPIB1–HPIB4** displayed a single emission band with maxima between 649 and 606 nm [649; **HPIB1**, 610; **HPIB2**, 606; **HPIB3** and 640 nm; **HPIB4**]. Among these **HPIB1** (λ_{em}; 649 nm) and **HPIB4** (λ_{em}; 640 nm) showed a large red shifted band relative to other compounds probably due to greater twisting.[29,30] Furthermore, the observed dihedral angles between the BODIPY core and phenyl ring **A** [Table 2: (80.93°; **HPIB1**, 61.85°; **HPIB2**, 60.68°; **HPIB3** and 71.22°; **HPIB4**) for these compounds clearly confirm our viewpoint. Other rings around imidazole also showed large dihedral angles with respect to the central imidazole ring for **HPIB1** and **HPIB4** confirming red-emission. Thus, it is concluded that the red-shift of emission maxima in the solid/aggregated state is related to the extent of twisting in the solid or crystalline state of the respective compounds.[29,30] Furthermore, it is worth noting that these compounds are good solid state emitters as a result of J-type molecular packing and the lack of detrimental π–π stacking as suggested by their crystal structures. It is observed that **HPIB1–HPIB4** displayed dual-emission in the aggregated state (in DMF/water mixtures at high f_w) compared to the apparent single emission band in the solid state. The dual-emission in the aggregated state is most probably due to conformation isomerization and it is presumed that two types of conformational isomers can exist in the DMF/water mixture due to single bond rotations. However, in the solid state only one conformer exists and shows a single emission band. Hence, from available data on **HPIB1–HPIB4** in the solid/aggregated state it can be concluded that emission behavior can be vastly tuned even by small structural changes in closely related molecules.

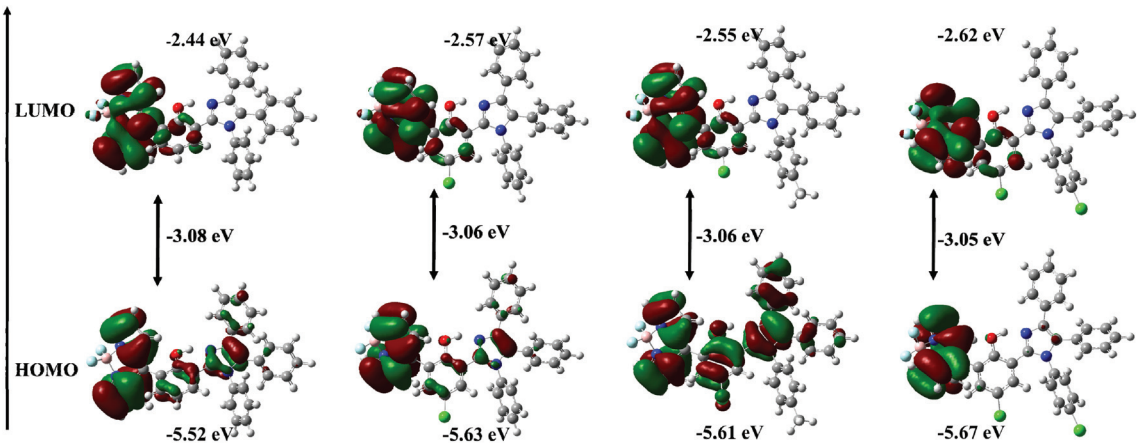

Fig. 12 Frontier molecular orbitals for **HPIB1–HPIB4**.

Theoretical considerations

To understand the orientation, photophysical properties and their correlation, DFT calculations have been performed on **HPIB1–HPIB4** using the B3LYP 6-31G** method (Fig. 12 and Fig. S53†). The orientation of DFT optimized structures resembles the orientation observed for the crystal structures. This has been confirmed by the comparison of the dihedral angles obtained from DFT optimized structures to those obtained from crystal structures (Table S7†). Furthermore, geometrical parameters like bond lengths and bond angles obtained from DFT optimized structures also showed good agreement with the structural data (Tables S5 and S6†). As depicted in Fig. 12, HOMO energy levels are spread over the phenyl-BODIPY core, imidazole and phenyl rings (attached to the imidazole), except for **HPIB4** wherein the HOMO is distributed only on the phenyl-BODIPY core, while the LUMO is mainly distributed over phenyl-BODIPYs. The HOMO–LUMO separations are almost similar (−3.08; **HPIB1**, −3.06; **HPIB2**, −3.06; **HPIB3** and −3.05 eV; **HPIB4**) and lie in the decreasing order from un-substituted (**HPIB1**) to substituted compounds (**HPIB4**). The energy difference lies in the descending order with increasing electron-withdrawing ability of $\mathbf{R_2}$ ($\mathbf{R_2}$; see Scheme 1). Furthermore, calculated electronic transitions (time-dependent DFT) are in good agreement with experimental results (Fig. S54 and Table S8†).

Conclusions

In summary, in this work, four novel hydroxyl-substituted tetraphenylimidazole (HPI) based BODIPYs displaying efficient AIE, solid state fluorescence, and greater sensitivity towards viscosity have been described. The twisted and non-planar orientation enables these systems to avoid π–π stacking and facilitates AIE behavior and solid state fluorescence. The efficient AIE of these derivatives has been related to J-aggregation in addition to RIRs. The phenyl rings of these derivatives enable them to act as FMRs due to the RIR process in viscous medium and therefore the systems become sensitive toward the viscosity of the medium and may find application in viscosity sensing. Theoretical data including electronic transitions deduced from DFT calculations for these derivatives match well with the experimental data. These HPI based BODIPYs displaying absorption and emission in the visible region [λ_{abs} ~505 nm, λ_{emi} ~535 nm (solution), λ_{emi} ~615 nm (aggregated state), and λ_{emi} ~649 nm (solid state)] may serve as good candidates for various applications including optoelectronics and sensing especially for biological purposes.

Conflicts of interest

The authors declare no conflict of interest.

Acknowledgements

The authors gratefully acknowledge the Science and Engineering Research Board (SERB), New Delhi, India for providing financial assistance through the scheme (EMR/2015/001535). B. K. D. acknowledges the University Grants Commission, New Delhi, India for a Senior Research Fellowship (22/6/2014(i)EU-V).

References

1 (*a*) S. C. Hong, D. P. Murale, M. Lee, S. M. Lee, J. S. Park and J.-S. Lee, *Angew. Chem., Int. Ed.*, 2017, **56**, 14642–14647; (*b*) D. Ding, K. Li, B. Liu and B. Z. Tang, *Acc. Chem. Res.*, 2013, **46**, 2441–2453; (*c*) R. P. Paitandi, V. Sharma, V. D. Singh, B. K. Dwivedi, S. M. Mobin and D. S. Pandey, *Dalton Trans.*, 2018, **47**, 17500–17514; (*d*) N. Guijarro, L. Yao, F. L. Formal, R. A. Wells, Y. Liu, B. P. Darwich, L. Navratilova, H.-H. Cho, J.-H. Yum and K. Sivula, *Angew. Chem., Int. Ed.*, 2019, **58**, 12696–12704; (*e*) G. Gupta, A. Das,

N. B. Ghate, T. Kim, J. Y. Ryu, J. Lee, N. Mandal and C. Y. Lee, *Chem. Commun.*, 2016, **52**, 4274–4277.

2 (*a*) J. B. Birks, *Photophysics of Aromatic Molecules*, Wiley, New York, 1970; (*b*) L. Peng, S. Xu, X. Zheng, X. Cheng, R. Zhang, J. Liu, B. Liu and A. Tong, *Anal. Chem.*, 2017, **89**, 3162–3168.

3 (*a*) J. Mei, N. L. C. Leung, R. T. K. Kwok, J. W. Y. Lam and B. Z. Tang, *Chem. Rev.*, 2015, **115**, 11718–11940; (*b*) J. Mei, Y. Hong, J. W. Lam, A. Qin, Y. Tang and B. Z. Tang, *Adv. Mater.*, 2014, **26**, 5429–5479; (*c*) Y. Kubota, K. Kasatani, H. Takai, K. Funabikia and M. Matsui, *Dalton Trans.*, 2015, **44**, 3326–3341; (*d*) J. Wang, A. Poirot, B. Delavaux-Nicot, M. Wolff, S. Mallet-Ladeira, J. P. Calupitan, C. Allain, E. Benoist and S. Fery-Forgues, *Dalton Trans.*, 2019, **48**, 15906–15916.

4 (*a*) Z. Zhang, C.-L. Chen, Y.-A. Chen, Y.-C. Wei, J. Su, H. Tian and P.-T. Chou, *Angew. Chem.*, 2018, **130**, 1–6; (*b*) Z. Zhao, Z. Wang, P. Lu, C. Y. K. Chan, D. Liu, J. W. Y. Lam, H. H. Y. Sung, I. D. Williams, Y. Ma and B. Z. Tang, *Angew. Chem., Int. Ed.*, 2009, **48**, 7608–7611; (*c*) G. R. Kumar, S. K. Sarkar and P. Thilagar, *Chem. – Eur. J.*, 2016, **22**, 17215–17225; (*d*) C. Arivazhagan, A. Maity, K. Bakthavachalam, A. Jana, S. K. Panigrahi, E. Suresh, A. Das and S. Ghosh, *Chem. – Eur. J.*, 2017, **23**, 7046–7051.

5 (*a*) S. Kaur, A. Gupta, V. Bhalla and M. Kumar, *J. Mater. Chem. C*, 2014, **2**, 7356–7363; (*b*) G. Feng, R. T. K. Kwok, B. Z. Tang and B. Liu, *Appl. Phys. Rev.*, 2017, **4**, 021307; (*c*) J. Luo, Z. Xie, J. W. Y. Lam, L. Cheng, H. Chen, C. Qiu, H. S. Kwok, X. Zhan, Y. Liu, D. Zhu and B. Z. Tang, *Chem. Commun.*, 2001, 1740–1741.

6 (*a*) H.-X. Yu, J. Zhi, T. Shen, W. Ding, X. Zhang and J.-L. Wang, *J. Mater. Chem. C*, 2019, **7**, 8888–8897; (*b*) S. Sasaki, G. P. C. Drummen and G.-i. Konishi, *J. Mater. Chem. C*, 2016, **4**, 2731–2743; (*c*) C. Zhang, Z. Han, M. Wang, Z. Yang, X. Ran and W. He, *Dalton Trans.*, 2018, **47**, 2285–2291.

7 V. S. Padalkar and S. Seki, *Chem. Soc. Rev.*, 2016, **45**, 169–202.

8 (*a*) F. Würthner, T. E. Kaiser and C. R. Saha-Möller, *Angew. Chem., Int. Ed.*, 2011, **50**, 3376–3410; (*b*) D. Tian, F. Qi, H. Ma, X. Wang, Y. Pan, R. Chen, Z. Shen, Z. Liu, L. Huang and W. Huang, *Nat. Commun.*, 2018, **9**, 2688; (*c*) S. Choi, J. Bouffard and Y. Kim, *Chem. Sci.*, 2014, **5**, 751–755.

9 (*a*) A. Loudet and K. Burgess, *Chem. Rev.*, 2007, **107**, 4891–4932; (*b*) T. Kowada, H. Maeda and K. Kikuchi, *Chem. Soc. Rev.*, 2015, **44**, 4953–4972; (*c*) P. E. Kesavan, S. Das, M. Y. Lone, P. C. Jha, S. Moric and I. Gupta, *Dalton Trans.*, 2015, **44**, 17209–17221; (*d*) C. Ray, J. Bañuelos, T. Arbeloa, B. L. Maroto, F. Moreno, A. R. Agarrabeitia, M. J. Ortiz, I. López-Arbeloab and S. d. l. Moya, *Dalton Trans.*, 2016, **45**, 11839–11848.

10 (*a*) D. Tleugabulova, Z. Zhang and J. D. Brennan, *J. Phys. Chem. B*, 2002, **106**, 13133–13138; (*b*) Y. Tokoro, A. Nagai and Y. Chujo, *Tetrahedron Lett.*, 2010, **51**, 3451–3454.

11 (*a*) T. T. Vu, M. Dvorko, E. Y. Schmidt, J.-F. Audibert, P. Retailleau, B. A. Trofimov, R. B. Pansu, G. Clavier and R. Méallet-Renault, *J. Phys. Chem. C*, 2013, **117**, 5373–5385; (*b*) J. R. Lakowicz, *Principles of Fluorescence Spectroscopy*, Springer, New York, 3rd edn, 2006.

12 (*a*) C. F. A. Gomez-Duran, R. Hu, G. Feng, T. Li, F. Bu, M. Arseneault, B. Liu, E. Penã-Cabrera and B. Z. Tang, *ACS Appl. Mater. Interfaces*, 2015, **7**, 15168–15176; (*b*) R. Hu, C. F. A. Gómez-Durán, J. W. Y. Lam, J. L. Belmonte-Vázquez, C. Deng, S. Chen, R. Ye, E. Peña-Cabrera, Y. Zhong, K. S. Wong and B. Z. Tang, *Chem. Commun.*, 2012, **48**, 10099–10101; (*c*) R. Hu, E. Lager, A. Aguilar-Aguilar, J. Liu, J. W. Y. Lam, H. H. Y. Sung, I. D. Williams, Y. Zhong, K. S. Wong, E. Peña-Cabrera and B. Z. Tang, *J. Phys. Chem. C*, 2009, **113**, 15845–15853; (*d*) H. T. Bui, D. K. Mai, B. Kim, K. H. Choi, B. J. Park and H. J. Kim, *J. Phys. Chem. B*, 2019, **123**, 5601–5607; (*e*) Z. Liu, Z. Jiang, M. Yan and X. Wang, *Front. Chem.*, 2019, **7**, 712; (*f*) J. Sturala, M. K. Etherington, A. N. Bismillah, H. F. Higginbotham, W. Trewby, J. A. Aguilar, E. H. C. Bromley, A.-J. Avestro, A. P. Monkman and P. R. McGonigal, *J. Am. Chem. Soc.*, 2017, **139**, 17882–17889; (*g*) Z. Xie, B. Yang, F. Li, G. Cheng, L. Liu, G. Yang, H. Xu, L. Ye, M. Hanif, S. Liu, D. Ma and Y. Ma, *J. Am. Chem. Soc.*, 2005, **127**, 14152–14153.

13 (*a*) S.-C. Lee, J. Heo, H. C. Woo, J.-A. Lee, Y. H. Seo, C.-L. Lee, S. Kim and O.-P. Kwon, *Chem. – Eur. J.*, 2018, **24**, 13706–13718; (*b*) P. S. Sherin, I. López-Duarte, M. R. Dent, M. Kubánková, A. Vyšniauskas, J. A. Bull, E. S. Reshetnikova, A. S. Klymchenko, Y. P. Tsentalovich and M. K. Kuimova, *Chem. Sci.*, 2017, **8**, 3523–3528; (*c*) M. K. Kuimova, G. Yahioglu, J. A. Levitt and K. Suhling, *J. Am. Chem. Soc.*, 2008, **130**, 6672–6673.

14 D. D. Perrin, W. L. F. Armango and D. R. Perrin, *Purification of Laboratory Chemicals*, Pergamon, Oxford, UK, 1986.

15 (*a*) G. M. Sheldrick, *SHELXL-97, Program for X-ray Crystal Structure Refinement*, Gottingen University, Gottingen, Germany, 1997; (*b*) G. M. Sheldrick, *SHELXS-97, Program for X-ray Crystal Structure Solution*, Gottingen University, Gottingen, Germany, 1997.

16 (*a*) A. L. Spek, *PLATON, A Multipurpose Crystallographic Tools*, Utrecht University, Utrecht, The Netherlands, 2000; (*b*) A. L. Spek, *Acta Crystallogr., Sect. A: Found. Crystallogr.*, 1990, **46**, C31.

17 (*a*) W. R. Wadt and P. Hay, *J. Chem. Phys.*, 1985, **82**, 284–298; (*b*) A. D. Becke, *J. Chem. Phys.*, 1993, **98**, 5648–5652.

18 M. J. Frisch, G. W. Trucks and H. B. Schlegel, *GAUSSIAN 09 Revision C. 01*, Gaussian Inc., Wallingford, CT, 2010.

19 S. Park, O.-H. Kwon, S. Kim, S. Park, M.-G. Choi, M. Cha, S. Y. Park and D.-J. Jang, *J. Am. Chem. Soc.*, 2005, **127**, 10070–10074.

20 B. K. Dwivedi, V. D. Singh, R. P. Paitandi and D. S. Pandey, *ChemPhysChem*, 2018, **19**, 2672–2682.

21 P. Thamyongkit, A. D. Bhise, M. Taniguchi and J. S. Lindsey, *J. Org. Chem.*, 2006, **71**, 903–910.

22 (*a*) A. Dvivedi, P. Rajakannu and M. Ravikanth, *Dalton Trans.*, 2015, **44**, 4054–4062; (*b*) S. Mukherjee and P. Thilagar, *Chem. – Eur. J.*, 2014, **20**, 9052–9062.

23 (*a*) R. S. Singh, S. Mukhopadhyay, A. Biswas and D. S. Pandey, *Chem. – Eur. J.*, 2016, **22**, 753–763; (*b*) B. K. Dwivedi, R. S. Singh, A. Ali, V. Sharma, S. M. Mobin and D. S. Pandey, *Analyst*, 2019, **144**, 331–341.

24 D. Li, X. Ni, X. Zhang, L. Liu, J. Qu, D. Ding and J. Qian, *Nano Res.*, 2018, **11**, 6023–6033.

25 (*a*) Y. Hong, J. W. Y. Lam and B. Z. Tang, *Chem. Commun.*, 2009, 4332–4353; (*b*) A. Maity, F. Ali, H. Agarwalla, B. Anothumakkool and A. Das, *Chem. Commun.*, 2015, **51**, 2130–2133.

26 (*a*) P. A. Kumar, A. H. Ashoka, M. Collot, A. Das and A. S. Klymchenko, *Chem. Commun.*, 2019, **55**, 6902–6905; (*b*) I. Lopez-Duarte, T. T. Vu, M. A. Izquierdo, J. A. Bull and M. K. Kuimova, *Chem. Commun.*, 2014, **50**, 5282–5284.

27 (*a*) S. Raut, J. Kimball, R. Fudala, H. Doan, B. Maliwal, N. Sabnis, A. Lacko, I. Gryczynski, S. V. Dzyuba and Z. Gryczynski, *Phys. Chem. Chem. Phys.*, 2014, **16**, 27037–27042; (*b*) M. Kaschke, J. Kleinschmidt and B. Wilhelmi, *Laser Chem.*, 1985, **5**, 119–132.

28 (*a*) G. A. Jeffrey, *An introduction to hydrogen bonding*, Oxford University Press, New York, 1997; (*b*) C. Zhu, A. U. Mu, Y.-H. Lin, Z.-H. Guo, T. Yuan, S. E. Wheeler and L. Fang, *Org. Lett.*, 2016, **18**, 6332–6335; (*c*) P. I. Nagy, *Int. J. Mol. Sci.*, 2014, **15**, 19562–19633.

29 (*a*) X. Zhang, Z. Chi, B. Xu, C. Chen, X. Zhou, Y. Zhang, S. Liu and J. Xu, *J. Mater. Chem.*, 2012, **22**, 18505–18513; (*b*) R. Hu, E. Lager, A. Aguilar-Aguilar, J. Liu, J. W. Y. Lam, H. H. Y. Sung, I. D. Williams, Y. Zhong, K. S. Wong, E. Peña-Cabrera and B. Z. Tang, *J. Phys. Chem. C*, 2009, **113**, 15845–15853; (*c*) P. Gopikrishna and P. K. Iyer, *J. Phys. Chem. C*, 2016, **120**, 26556–26568.

30 S. B. Anantharaman, S. Yakunin, C. Peng, M. V. G. Vismara, C. F. O. Graeff, F. A. Nüesch, S. Jenatsch, R. Hany, M. V. Kovalenko and J. Heier, *J. Phys. Chem. C*, 2017, **121**, 9587–9593.